Sphingomyelin is critical in organizing phosphoinositide dynamics during phagocytic uptake of *Mycobacterium tuberculosis*

Patrick Niekamp[2], Gaelen Guzman[1], Hans Leier[1], Ali Rashidfarrokhi[3], Veronica Richina[4], Joost Holthuis[2], Fikadu G. Tafesse[1]*

[1]Department of Molecular Microbiology and Immunology, Oregon Health & Science University, 3181 SW Sam Jackson Park Road, Portland, OR 97239.

[2]Biology & Chemistry Department, University of Osnabrück, Fachbereich Biologie/Chemie, Barbarastrasse 13, 49076 Osnabrück, GERMANY.

[3]Department of Pathology and Department of Medicine, New York University Langone, 550 First Avenue, MSB 594, New York, NY 10016.

[4]Ragon Institute of MGH, MIT, and Harvard, 400 Technology Square, Cambridge, MA 01239-7000.

*Communicating Author: tafesse@ohsu.edu

Abstract

Infection by *Mycobacterium tuberculosis* (Mtb) represents a significant global health burden. Mtb invades alveolar macrophages through phagocytosis, and cholesterol has been shown as essential for this invasion, but the roles played by other host lipids have remained unstudied. As such, this study aimed to explore the manners in which host sphingolipids play roles in the early stages of Mtb infection. To this end, we use chemical and genetic perturbations of the sphingolipid biosynthetic pathway and fluorescence microscopy to show that sphingolipids are required for efficient phagocytosis of Mtb. We isolate this dependency to the presence of sphingomyelin at the cell

surface. We furthermore show that the turnover dynamics of phosphoinositides at the phagosomal synapse are perturbed upon blockade of sphingolipid synthesis. Finally, we show that the aggregation of membrane-bound receptor at the phagocytic synapse is defective in sphingolipid-deficient cells. This work represents an essential step in understanding the coalescence of host-pathogen interactions that give rise to Mtb as a global pathogen.

Introduction

The etiologic agent behind an estimated 10 million new cases of tuberculosis and 1.6 million deaths in 2017 alone, *Mycobacterium tuberculosis* (Mtb) has established itself as a highly insidious pathogen[1,2]. Mtb invades alveolar immune cells through phagocytosis, and wields an extensive repertoire of effector molecules that operate to dampen the immune response, reprogram the host lipidome, and promote long-term intracellular survival[3,4]. As an intracellular pathogen, Mtb necessarily interacts with its host along numerous lipid interfaces throughout its infectious lifecycle – and understanding the roles played by host lipids at the site of phagocytic invasion may illuminate novel routes of therapeutic strategies to prevent the onset and spread of tuberculosis[5].

In most contexts, phagocytosis is critical for clearing dead and effete cells, and serves as a first line of defense against pathogens such as bacteria, parasites, and fungi. This process culminates in the engulfment and internalization of target particles, which are subsequently degraded via convergence of the phagosome with the lysosome[6]. In the context of pathogen clearance, uptake by professional phagocytes (primarily monocytes, macrophages, and dendritic cells) results in robust inflammatory response and presentation of pathogen-derived antigens to the adaptive immune compartment – thereby acting as a critical component of the immune response to infections[7]. For example, previous work shows that phagocytic uptake of *Candida albicans* is essential

for the clearance of infection *in vivo*[8]. However, Mtb is highly adept at subverting its own degradation to survive within phagosome-derived compartments. Among many known mechanisms of host cell manipulation, this pathogen has been shown to interfere with Ca^{2+}-induced maturation of the phagosome through disruption of sphingosine kinase activity, which produces the potent signaling molecule sphingosine-1-phosphate[6,9]. However, the specific functional roles played by host lipid species at the site of initial phagocytic uptake of Mtb have remained relatively unstudied. In particular, the structural and signaling functions played by sphingolipids at the cell membrane and within the phagosome during Mtb infection are unknown.

Sphingolipids are a complex family of membrane lipids that contain a sphingoid base. A growing body of literature shows that sphingolipids mediate functions beyond membrane barrier components: members of this family accumulate in lipid rafts and act as secondary messengers within the cell[10–12]. These signaling functions are relevant to many biological processes that span from apoptosis and autophagy to stress response and inflammation[13–15]. Notably, it has been shown that the biosynthetic flow of sphingolipids through the Golgi creates a regulatory feedback loop that controls the levels of phosphatidylinositol4-phosphate – though interactions outside of the trans-Golgi network are unknown[16]. Of interest to a study on phagocytosis, sphingomyelin constitutes a significant fraction of the total lipid composition of the exoplasmic leaflet of the plasma membrane and plays critical roles in the organization of lipid rafts[17,18].

Prior work has investigated the roles played by sphingolipids during the phagocytosis of other particles – there exist contradictory reports describing the effect of sphingolipid depletion during phagocytosis. In one example, we have previously reported that cellular sphingolipids are critical for the clearance of *Candida albicans* through phagocytosis by macrophages[8]. In another

contrasting example, depletion of cellular sphingolipids has also been reported to enhance phagocytic uptake of opsonized particles. Together, these differing results suggest that the roles played by sphingolipids during phagocytosis may be pathogen or particle specific, based on the specific ligands decorating a particle[19]. The role of sphingolipids during uptake of Mtb is unknown. However, it has been shown previously that phagocytosis of Mtb is cholesterol-dependent[20].

Here, we employed chemical and genetic tools to manipulate the levels of sphingolipids in mammalian phagocytes, and infected using an mCherry-expressing reporter strain of H37Rv Mtb. We find a role for sphingolipids in Mtb phagocytosis. We show that sphingolipid-depleted cells display defects in phagocytic signaling including a defect in recruitment of the small GTPases Rac1 and CD42 to the phagocytic up. We further show that phosphoinositide dynamics upon engagement of phagocytic particles is impaired in sphingolipid depleted cells. Together, these data suggest a novel mechanism through which sphingolipids coordinate phosphoinositide-mediated signaling during phagocytosis of Mtb.

Results

Manipulating sphingolipid biosynthesis in mammalian phagocytes using chemical and genetic tools.

To answer our central question – "Are sphingolipids required for the phagocytic uptake of Mtb?" – we sought mechanisms for inhibiting the biosynthesis of sphingolipids in a cohort of model phagocytes. We first used a chemical approach to inhibition using the compounds myriocin and fumonisin B1. As depicted in Figure 1a, the initial and rate limiting step of sphingolipid synthesis is the production of the sphingoid base through the condensation of Serine and palmitoyl-

CoA, and is performed by the enzymatic complex serine palmitoyltransferase (SPT)[21]. The atypical amino acid myriocin (Myr) specifically blocks the activity of SPT, and thereby ablates total *de novo* synthesis of sphingolipids[8]. The fungal toxin fumonisin B1 (FB1) acts several steps downstream in the sphingolipid biosynthetic pathway, and blocks the activity of ceramide synthase[8]. Ceramide acts as a central nexus in the sphingolipid population – it is converted into many classes of higher sphingolipids, including sphingomyelin, glycosphingolipids, and galactosylceramides[22,23].

To verify the reported effects of myriocin and fumonisin B1, we used thin layer chromatography to visualize the incorporation of 3-L-[^{14}C]-serine into sphingolipid species in RAW 246.7, THP-1, DC 2.4, and U937 cells following 3-day treatment with 15 μM Myr and 5μM FB1 (Figure 1d and Supplementary Figure 1). Across all cell lines, treatment with these compounds result in a significant reduction in sphingolipid content, whereas phosphatidylserine content is unaffected – demonstrating the specificity and potency of these compounds.

As an orthogonal method to the above chemical inhibitors, we used CRISPR/Cas-9 editing to generate Sptlc2 knockouts in both RAW 264.7 and DC 2.4 cells. Sptlc2 is one of the three members of the SPT complex, and we have previously reported its loss to mirror Myr treatment[8]. We validated loss of protein expression by Western blotting (Figure 1c). We again used thin layer chromatography to visualize the incorporation of 3-L-[^{14}C]-serine into lipid species in both wildtype and Sptlc2-/- RAW 246.7 and DC 2.4 cells. We show significant reduction of sphingolipid content in these knockout cells, and no effect on phosphatidylserine content (Figure 1e,f and Supplemental Figure 1).

As further examination of the lipid composition of sphingolipid deficient cells, we performed mass spectroscopy-based lipidomic analysis of RAW 264.7 macrophages following treatment with chemical inhibitors and Sptlc2 knockout. By examining cellular levels of sphingosine, ceramide, sphingomyelin, and glucosylceramide, we hoped to gain granular insight into the effects of these inhibitor treatments and genetic knockout. As expected, both myriocin and Sptlc2 knockout result in significant reduction of all sphingolipid species, and no change to phosphatidylcholine levels (Figure 1 g-j and data not shown). In fumonisin B1 treated cells, we observe reduction of all sphingolipid species downstream of ceramide synthesis (the point of inhibition along the biosynthetic pathway), but we observe a concordant increase in sphingosine (synthesized upstream of ceramide), as reported previously (Figure 1g-j)[24]. We observe a decrease in phosphatidylcholine levels following treatment with FB1 – suggesting that this molecule may result in off-target effects on lipid synthesis (data not shown). Keeping in mind the caveat of these off-target effects, we included FB1 in our cohort of mechanisms for inhibiting sphingolipid biosynthesis.

Notably, we observe that myriocin and fumonisin B1 treatment, as well as Sptlc2 knockout, do not result in the total ablation of cellular sphingolipid content. This is at least partially attributable to the activity of the sphingolipid salvage pathways, through which cells may acquire sphingolipids from additives in media (primarily fetal calf serum). As we describe below, cells grown in the absence of serum additive quickly die when sphingolipid biosynthesis is inhibited.

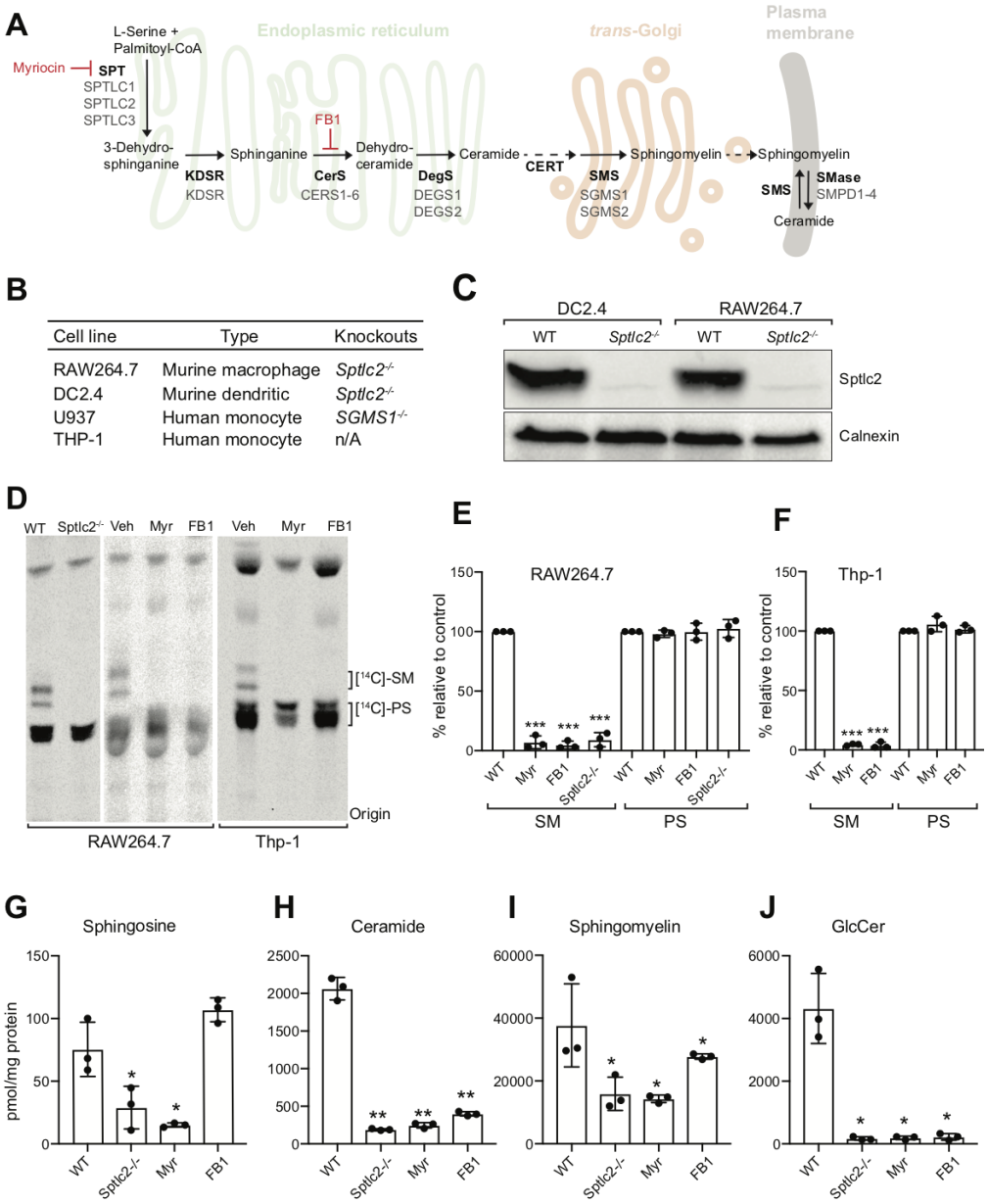

Figure 1: *Cellular sphingolipid levels may be manipulated using chemical and genetic tools.*
Summary of effects of chemical and genetic tools used to manipulate cellular sphingolipid biosynthesis. (A) Simplified overview of sphingolipid biosynthetic pathway. (B) Model phagocyte cell lines used in this study, respective species background, and genetic knockouts available. (C) Western blot probed using anti-Sptlc2 antibody in wildtype and CRISPR/Cas-9 knockout DC 2.4 and RAW 264.7 cells (upper), and probed against calnexin as loading control (lower). (D) Thin layer chromatography after radioactive labeling with 3-L-[^{14}C]-serine in the following cell conditions: RAW 264.7 wildtype and Sptlc2-/- cells; RAW wildtype cells following three-day treatment with vehicle control, 5μM myriocin, or 15μM fumonisin B1; and THP-1 wildtype cells following three-day treatment with vehicle control, 5μM myriocin, or 15μM fumonisin B1. (E) Quantification of RAW 264.7 lanes of TLC shown in D. Left bars depict sphingomyelin content (SM), right bars depict phosphatidylserine content (PS). (F) Quantification of THP-1 lanes of TLC shown in D. Left bars depict SM content, right bars depict PS content. (G-J) Lipidomics analysis of several sphingolipid species of interest isolated from RAW 264.7 cells of the following conditions: wildtype (no treatment), Sptlc2-/-, three-day treatment with 5μM myriocin, and three-day treatment with 15μM fumonisin B1. An unpaired Student's T-test was used to compare sphingolipid content between wildtype/untreated cells and mutant/treated cells. NS = not significant, *p<0.05, **p<0.01, ***p<0.001.

Sphingolipid depletion has no effect on cell morphology or cell division.

What effect does the inhibition of sphingolipid synthesis have on basal cellular functions? We hoped to characterize the changes to morphology and cell growth resulting from myriocin and fumonisin B1 treatments, and Sptlc2 knockout.

We show that in RAW 264.7, DC 2.4, THP-1, and U937 cells, there are limited decreases in cellular replication following four-day treatments with 5μM myriocin and 15μM fumonisin B1, and following Sptlc2 knockout (Supplementary Figure 2b,c and data not shown). Similarly, we use brightfield microscopy to show that there are no obvious defects of cellular morphology over the course of inhibitor treatments, or following Sptlc2 knockout (Supplementary Figure 2a and data not shown). As noted above, fetal calf serum is an essential additive when culturing sphingolipid-deficient cells. We observe that RAW 264.7 Sptlc2 knockout cells rapidly die in the absence of serum, whereas wildtype cells remain relatively healthy after three days without serum (data not shown). We believe that cells deficient in sphingolipid biosynthesis acquire sphingolipids from media at only the minimal level to allow cell growth, as their overall sphingolipid content is significantly lower than in wildtype cells.

Notably, when grown in the presence of fetal calf serum, the major phenotype observed in these cells over the course of this study is in the rate of phagocytic uptake of certain particles, as we have reported previously for DC 2.4 knockout cells[8]. We observe that RAW 264.7 cells display a three-fold reduction in the capacity to phagocytose Zymosan A particles (data not shown).

Having thus characterized the effects inhibition of sphingolipid biosynthesis, we hoped to use these inhibitory mechanisms (myriocin, fumonisin B1, and Sptcl2 knockout) to address the question: “Are sphingolipids an essential host factor in the phagocytic uptake of *Mycobacterium tuberculosis*?”

***Cells deficient in sphingolipid biosynthesis are reduced in the capacity to phagocytose* Mtb.**

To investigate the role of sphingolipids during phagocytic uptake of Mtb, we used Myr and FB1 to block sphingolipid synthesis in, RAW 264.7, THP-1, DC2.4, and U937 cells. We then infected cells with an mCherry-expressing strain of Mtb to quantify rates of phagocytosis. Briefly, cells were infected at a multiplicity of infection (MOI) of 10 for two hours, after which cells were fixed and stained with Alexa Fluor 488-conjugated phalloidin and with DAPI (to visualize F-actin at cell boundary and nuclei, respectively). Fluorescence microscopy was used to quantify uptake efficiency through automated counting of cell number (by nuclei) and internalized bacteria (red fluorescent particles within green cell boundary). We report uptake efficiency as the ratio of the total number of internalized Mtb particles against the number of identified nuclei, and normalized the uptake rate of treated cells to that of untreated cells to compensate for variability between biological replicates. In all cell models analyzed, we observed a statistically significant reduction in Mtb uptake of approximately 50% following treatment with myriocin, and approximately 40% for fumonisin B1 (Figure 2a-h). Similarly, the knockout of Sptlc2 resulted in approximately 50% of wildtype uptake in both RAW 264.7 and DC 2.4 cells (Figure 2a-h).

These results suggest that the maintenance of total cellular sphingolipid levels through active sphingolipid biosynthesis is required for efficient uptake of Mtb across four model cell lines and irrespective of the mechanism of inhibition. We next hoped to identify the exact species required for efficient Mtb uptake.

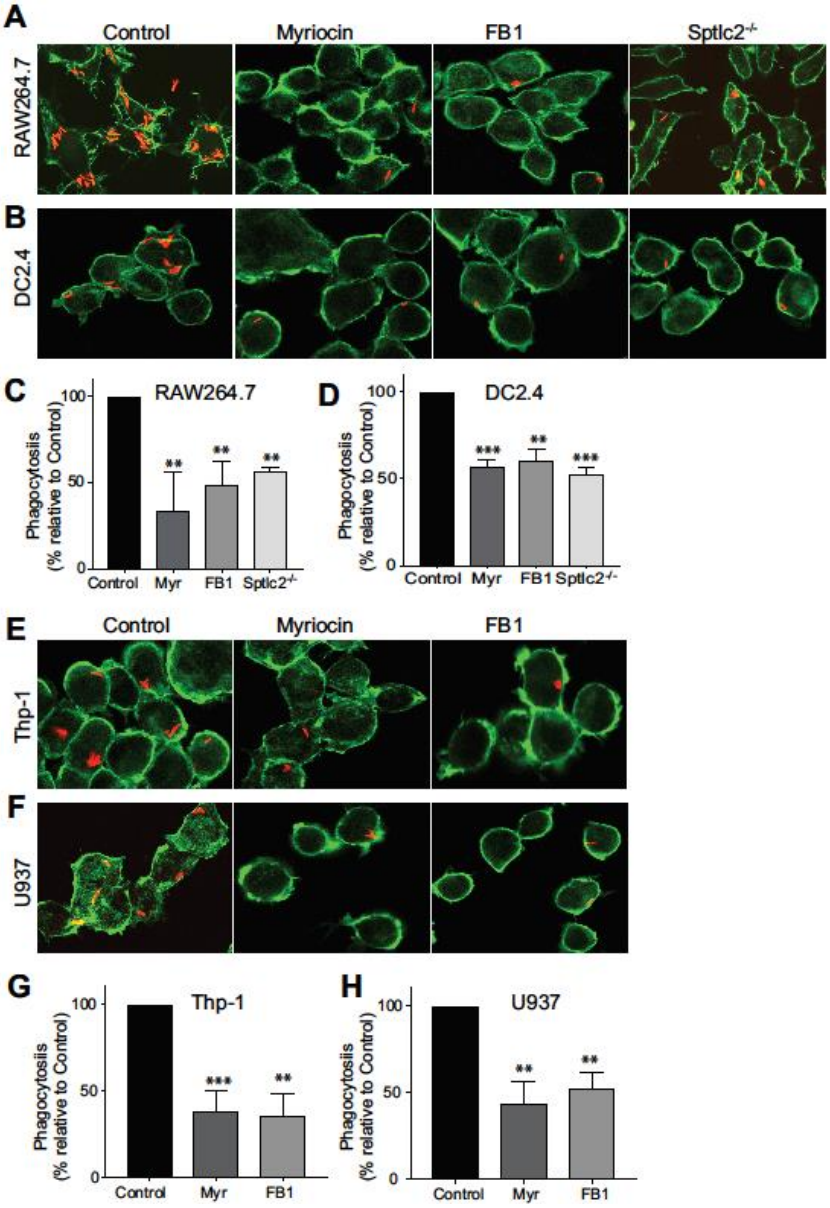

Figure 2: *Sphingolipid biosynthesis is required for efficient phagocytosis of Mtb.*

Uptake assays following infection of sphingolipid-deficient cells with mCherry-expressing Mtb. Briefly, cells were infected at MOI of 10 for 2 or 4 hours at 37°C and 5% CO_2, fixed overnight, and stained with Phalloidin-Alexa488. Representative confocal images were collected at 63x, and non-confocal quantitative images were collected at either 40x or 10x. (A and B) Representative images of Mtb-infected RAW 264.7 and DC 2.4 cells. Three days prior to infection, wildtype cells were plated in a 6-well plate and left untreated or treated with 5μM myriocin or 15μM fumonisin B1. One day prior to infection, $2x10^4$ Sptlc2-/- and untreated/treated wildtype cells were plated in parallel in a 96-well plate and respective treatments were continued. (C and D) Quantification of Mtb uptake in RAW 264.7 and DC 2.4 cells over three independent biological replicates, with at least 1000 cells quantified per replicate, +/- standard deviation. Mtb uptake was defined using total number of bacteria (mCherry signal) within cellular periphery (Phalloidin-Alexa488 signal) and cellular counts were defined by nuclear stain. (E and F) Representative images of infected THP-1 and U937 monocyte-derived macrophages. $2x10^4$ THP-1 and U937 cells were plated in 96-well plate and were differentiated using 80ng/ml PMA for one day, and then treated for three days with 5μM myriocin or 15μM fumonisin B1. (G+H) Quantification of Mtb uptake in THP-1 and U937 cells over three independent biological replicates, with at least 1000 cells quantified per replicate, +/- standard deviation. An unpaired Student's T-test was used to compare Mtb uptake between wildtype/untreated cells and mutant/treated cells. NS = not significant, *p<0.05, **p<0.01, ***p<0.001.

Sphingolipid depleted cells are defective in activation of small GTPases Cdc42/Rac1.

What is the mechanism through which sphingolipids enable phagocytic uptake of Mtb? Phagocytosis is strictly regulated through a signaling network that involves the dynamic activation and recruitment of both enzymes (such as GTPases, kinases, and phosphatases) and lipids – particularly several phosphatidylinositol species (Figure 3a). During the phagocytosis of pathogenic particles, Mtb included, the primary GTPases of action are Cdc42 and Rac1[25]. These two GTPases are activated through phosphorylation following engagement of particle and aggregation of receptor, and this activation builds as a particle is fully engaged by phagocytic receptor. Once a particle is engulfed, the phagocytic signaling cascade is terminated by the dephosphorylation of Cdc42 and Rac1[25]. We hypothesized that inhibiting sphingolipid biosynthesis would prohibit the activation of Cdc42 and Rac1 during phagocytosis.

To address this hypothesis, we transfected wildtype and Sptlc2-/- RAW 264.7 macrophages with a fluorescent biosensor consisting of the p21 binding domain of the p21 activated kinase, fused to YFP (PBD(PAK)-YFP) – which is recruited from the cytosol to specifically bind to phosphorylated Cdc42 and Rac1 at the site of phagosome formation[26,27]. We then infected cells using the phagocytic model particle Zymosan A at an MOI of 10 for short timepoints before performing live imaging to track the localization of these GTPases.

Due to the BSL3 requirements of Mtb, we used the model phagocytic particle Zymosan A in these live imaging experiments. Zymosan A particles are composed of chains of fungus-derived β-glucan – which engages the mannose receptor on professional phagocytes[28]. We have observed that sphingolipid depletion reduces uptake of Zymosan A to a similar degree as to Mtb (data not shown). Established literature suggests that Dectin-1 is a major phagocytic receptor engaged by Mtb during infection, though the exact epitope of Dectin-1 recognition is not known[29,30].

We first demonstrate in wildtype RAW 264.7 cells that Cdc42/Rac1 activity builds upon particle recognition and peaks as a particle is engulfed (Figure 3b and Supplementary Movie 1). Quantifying the enrichment of reporter signal to the site of particle contact versus cytosol signal across at least four cells shows a sharp peak of biosensor recruitment as a particle is engulfed (Figure 3c). In contrast, this activation initially builds in Sptlc2-/- cells at a rate indistinguishable from wildtype, but Cdc42/Rac1 activity fails to continue accumulating at later timepoints (Figure 3b+c and Supplementary Movie2).

From these results, we conclude that in sphingolipid-deficient cells, the initial activation of Cdc42/Rac1 are unaffected – but that this activation fails to peak at high enough levels to fully engulf pathogen-particles. The initial stages of phagocytosis briefly act in a sort of positive feed-back loop, in which the engagement of receptor initiates signaling that results in the additional aggregation of receptor and thus further enhances signal. Because the initial stages of phagocytosis are unaffected by deficient biosynthesis of sphingolipids, we hypothesized that an intermediate signaling step is dependent on sphingolipid levels at the cell membrane. We next hoped to charac-terize the activity of downstream phosphoinositide signaling to explain this observation.

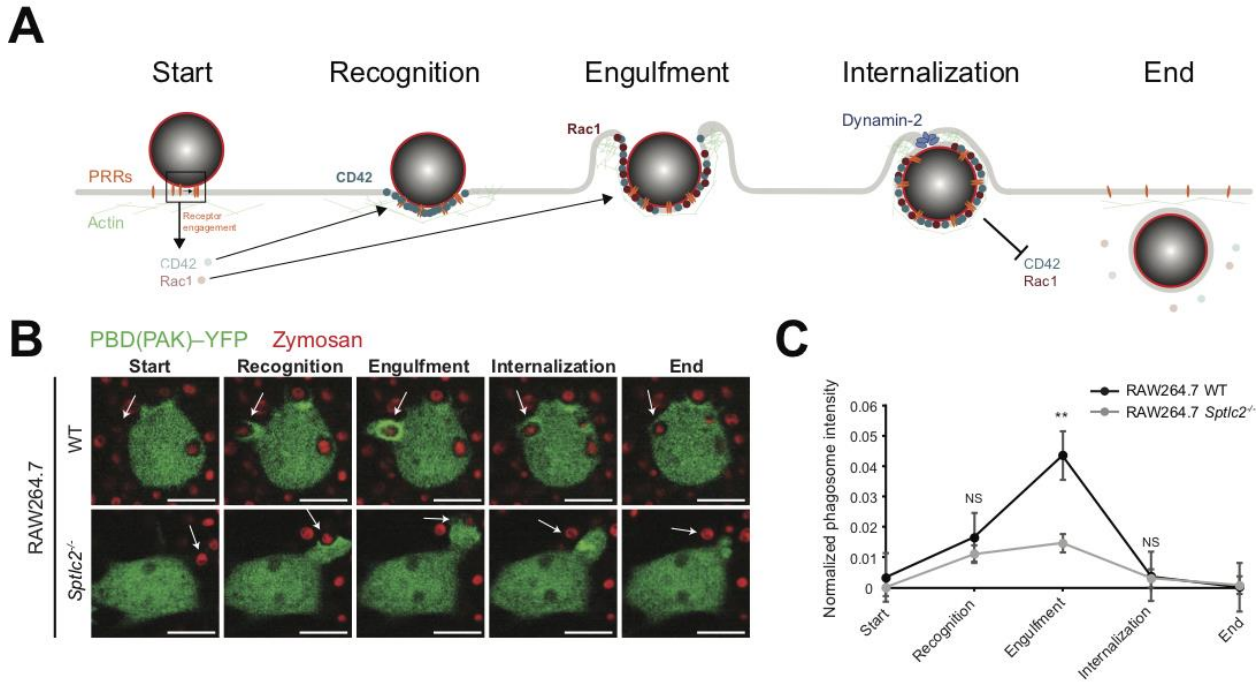

Figure 3: *Accumulation of activated Cdc42 and Rac1 is defective in sphingolipid-deficient cells.*

Assessment of Rho GTPase activity in sphingolipid-deficient cells during phagocytosis. (A) Depiction of Cdc42 and Rac1 activation and deactivation at the phagosome following receptor engagement and particle engulfment. (B) Time-lapse spinning-disk confocal microscopy images of wildtype and Sptlc2-/- RAW 264.7 cells after infection with Zymosan A particles at MOI 20. Briefly, cells were transiently transfected with PBD(PAK)-YFP biosensor 24-hours before infection; immediately before imaging, growth medium was replaced with Alexa594 Zymosan A resuspended in RPMI without phenol red. (C) Accumulation of YFP signal to site of particle binding was quantified by the ratio of YPF signal intensity at phagosome versus YFP signal across entire cell at five indicted time points. The mean YFP intensity profiles of at least four cells are represented +/- standard deviation. NS = not significant, *p<0.05, **p<0.01, ***p<0.001.

Sphingolipid depleted cells are defective in phosphatidylinositol 3,4,5-*tris*phosphate synthesis.

Do sphingolipids mediate phosphoinositide signaling during phagocytosis? Rho GTPase activation initiates the conversion of phosphatidylinositol 4-phosphate ($PI_{(4)}P$) to phosphatidylinositol 4,5-*bis*phosphate ($PI_{(4,5)}P_2$) at the base of the phagocytic synapse; this buildup of $PI_{(4,5)}P_2$ is essential to initiate the polymerization of actin filaments that drive the leading edges of the growing phagosome around the particle (Figure 4a)[27]. Following the leading edge of $PI_{(4,5)}P_2$ production, the enzyme phosphatidylinositol 3-kinase (PI_3K) converts $PI_{(4,5)}P_2$ into phosphatidylinositol 3,4,5-*tris*phosphate ($PI_{(3,4,5)}P_3$), which produces a trailing edge of actin disassembly at the base of the phagosomal cup – critical for the engulfment of the engaged particle[7]. To date, there have been no reports connecting phosphoinositide signaling to sphingolipids during phagocytosis, but previous work has established a feedback circuit in which sphingolipid synthesis regulates phosphoinositide dynamics within the Golgi[16,31]. As such, we hypothesized that sphingolipids play a similar role in phosphoinositide turnover during phagocytosis of Mtb-like particles.

To address this hypothesis, we transfect RAW 264.7 wildtype and Sptlc2 knockout cells with biosensors that specifically bind to two phosphoinositide species and use live imaging to assess the uptake of Zymosan A particles. The first biosensor we used consisted of the fusion of GFP to the plekstrin homology (PH) domain of phospholipase C-delta (PLCδ), which selectively binds to $PI_{(4,5)}P_2$[7]. We show that wildtype cells synthesize $PI_{(4,5)}P_2$ following the recognition of a phagocytic particle, and that this synthesis peaks with the engulfment of the particle (Figure 4b+c and Supplemental Movie 3). In Sptlc2 knockout cells, $PI_{(4,5)}P_2$ production is initially the same as in wildtype cells, but fails to build to the same levels as the cells fail to uptake particles (Figure 4b+c and Supplementary Movie 4).

Next, we transfected RAW 264.7 cells with a $PI_{(3,4,5)}P_3$ biosensor consisting of the PH domain of Akt fused to GFP (PH(AKT)-GFP)[32]. We use this biosensor construct to show that wildtype cells begin synthesizing $PI_{(3,4,5)}P_3$ early in phagocytosis, but that this synthesis strongly peaks as a particle is fully engulfed (Figure 4f+g and Supplementary Movie 5). However, Sptlc2 knockout cells fail to produce a trailing wave of $PI_{(3,4,5)}P_3$, and thus never reach the levels of synthesis observed in wildtype cells (Figure 4f+g and Supplementary Movie 6).

Together, these findings suggest that the inefficiency of Mtb uptake in sphingolipid-deficient cells is due to defects in phagocytic signaling resulting from defective phosphoinositide dynamics. At early stages of phagocytosis, there are minimal differences between wildtype and Sptlc2-/- cells – but the knockout cells fail to reach critical thresholds of phosphoinositide signal molecules (particularly $PI_{(3,4,5)}P_3$) to drive the full propagation of phagocytosis and thereby fail to uptake particles.

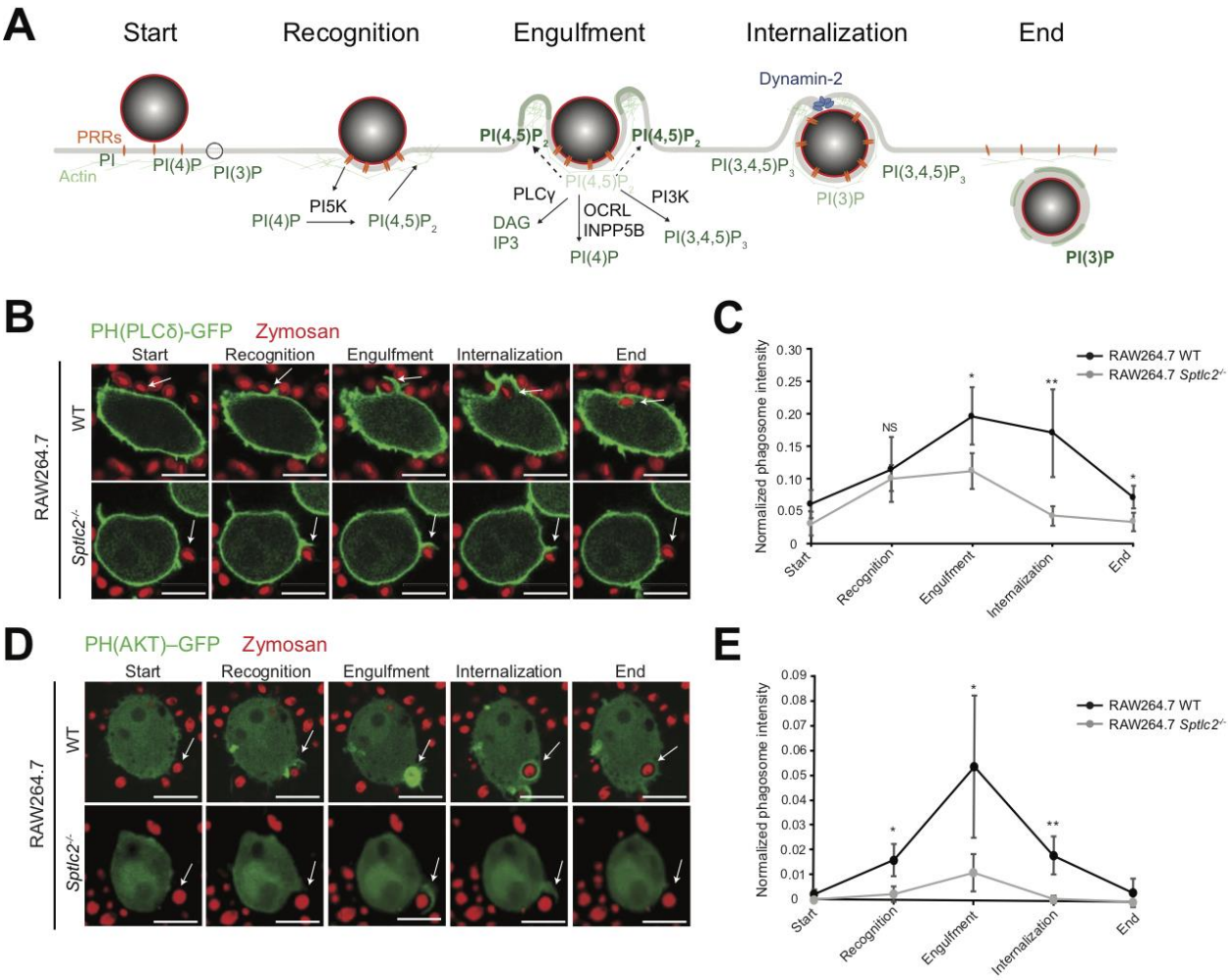

Figure 4: *Phosphoinositide turnover dynamics are disrupted in sphingolipid-deficient phagocytes.*

(A) Depiction of phosphoinositide dynamics during phagocytosis. (B+D) Time-lapse spinning-disk confocal microscopy images of wildtype and Sptlc2-/- RAW 264.7 cells after infection with Zymosan A particles at MOI 20. Briefly, cells were transiently transfected with either PH(PLCδ)-GFP or PH(AKT)-GFP biosensors 24-hours before infection (in B and D, respectively); immediately before imaging, growth medium was replaced with Alexa594 Zymosan A resuspended in RPMI without phenol red. (C+E) Accumulation of GFP signal to site of particle binding was quantified by the ratio of GPF signal intensity at phagosome versus GFP signal across entire cell at five indicted time points. The mean GFP intensity profiles of at least four cells are represented +/- standard deviation. NS = not significant, *p<0.05, **p<0.01, ***p<0.001.

Sphingomyelin in particular is required for efficient uptake of Mtb.

Which sphingolipid confers this phenotype? Because sphingomyelin is highly enriched to the exoplasmic leaflet of the plasma membranes, we hypothesized that this lipid species is responsible for the observed phenotype of reduced Mtb uptake in cells depleted of total sphingolipids[17,22,33]. Because sphingomyelin is a terminal branch of the sphingolipid biosynthetic pathway, and its synthesis at the plasma membrane is mediated by the enzyme sphingomyelin synthase 1 (Sgms1), cells may be depleted of this specific lipid species through CRISPR/Cas9-mediated knockout of this gene. We isolated two U937 Sgms1 knockout clones and assessed their capacity to phagocytose Mtb through infection as described above. We found that, despite minor clonal differences, these cells are significantly reduced in their capacity to uptake Mtb to a similar degree as to cells deficient in the biosynthesis of all sphingolipids (Figure 5a+b).

Together with the above results, these data suggest that sphingomyelin is particularly crucial for the phagocytic uptake of particles such as Mtb.

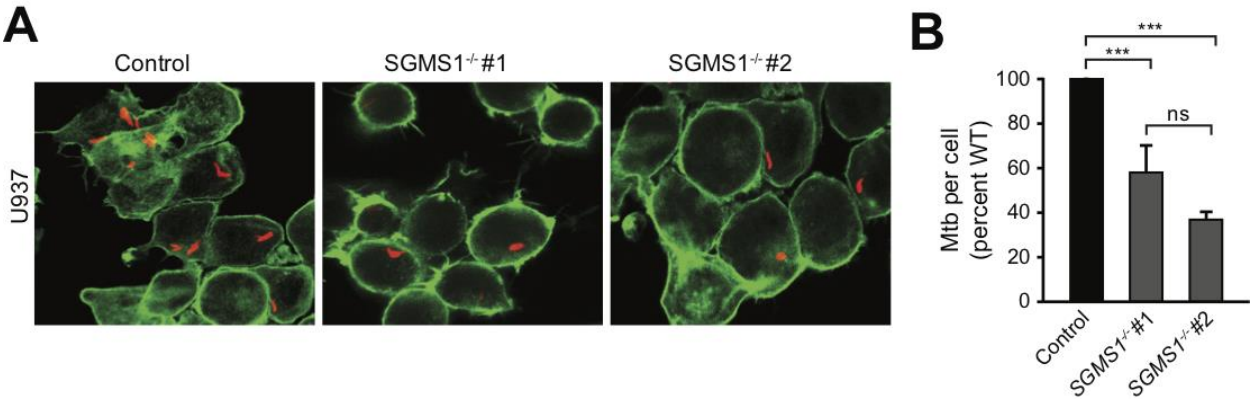

Figure 5: *Blockade of sphingomyelin synthesis mimics inhibition of total sphingolipid biosynthesis.* Uptake assays following infection of Sgms1-/- U937 cells with mCherry-expressing Mtb. Briefly, cells were infected at MOI of 10 for 2 or 4 hours at 37°C and 5% CO_2, fixed overnight, and stained with Phalloidin-Alexa488. Representative confocal images were collected at 63x, and non-confocal quantitative images were collected at either 40x or 10x. (A) Representative images of infected U937 monocyte-derived macrophages of wildtype background, and of two isolated clones of Sgms1 CRISPR knockouts. $2x10^4$ U937 cells were plated in 96-well plate and differentiated using 80ng/ml PMA for one day, and then treated for three days with 5µM myriocin or 15µM fumonisin B1. (B) Quantification of Mtb uptake in wildtype and Sgms1-/- U937 cells over three independent biological replicates, with at least 1000 cells quantified per replicate, +/- standard deviation.

The phagocytic receptor Dectin-1 fails to aggregate at the site of particle engagement.

As described by Goodridge et al. in 2011, the engagement of phagocytic receptor to ligand initiates the accumulation of receptor to the phagocytic synapse – resulting in the physical rejection of inhibitory phosphatases from the phagocytic synapse and the formation of a lipid raft-like domain[34]. Prior work has shown that the several intracellular pathogens, including Mtb, induce their uptake in a cholesterol-dependent manner[5,35]. As such, we hypothesized that cellular sphingolipid content is required for the proper aggregation of the phagocytic receptor Dectin-1 to the site of particle engagement.

To address this hypothesis, we transiently transfected wildtype and Sptlc2-/- RAW 264.7 macrophages with a GFP-conjugated Dectin-1 construct, and assessed the co-localization of this fluorescent protein with Zymosan A particles at short timepoints. We find that Dectin-1 in wildtype cells strongly accumulates at the site of contact with Zymosan A, and that this contact area spreads with the engulfment of the particle (Figure 6a+b). In contrast, Sptlc2 knockout cells fail to accumulate Dectin-1 at the site of engagement (Figure 6c+d). We believe that this failure to aggregate phagocytic receptor suggests that fluidity at the phagocytic synapse is significantly perturbed by the depletion of sphingolipids.

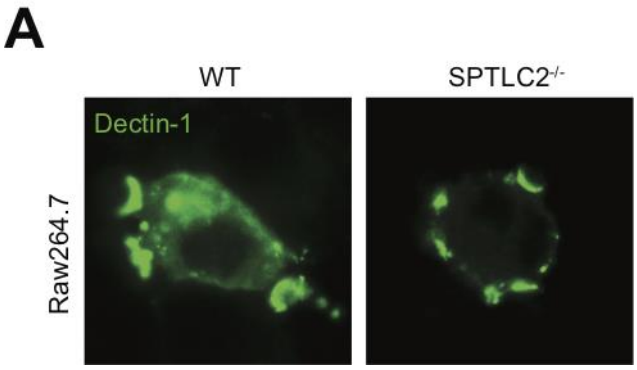

Figure 6: *Phagocytic receptor Dectin-1 fails to aggregate at phagosome in sphingolipid deficient cells.* Visualization of Dectin-1-GFP localization following infection with Alexa594-conjugated Zymosan A at MOI 10. Wildtype and Sptlc2-/- RAW 264.7 cells were plated on glass coverslips and transiently transfected with Dectin-1-GFP 48-hours prior to infection. Growth media was aspirated, and Zymosan A solution in RPMI was added to cells. Infected cells were incubated for 5 minutes at 37°C and fixed in 4% paraformaldehyde. (A) Confocal microscopy of Alexa594-Zymosan A-infected wildtype and Sptlc2-/- RAW 264.7 macrophages.

Discussion

In this study, we report that the capacity of Mtb to invade host cells by engagement of phagocytic receptors is significantly dependent on the active biosynthesis of host sphingolipids at the cell membrane. Our three central findings are thus: First, the blockade of total sphingolipid synthesis reduces Mtb uptake by approximately 50% – and the specific blockade of sphingomyelin synthesis produces a phenocopy of this observation. Next, we show that several critical stages of phagocytic signaling involving phosphoinositide dynamics are perturbed upon depletion of sphingolipid synthesis, resulting in defective phagosome formation. And finally, we show that the aggregation of phagocytic receptor is defective in sphingolipid-deficient cells.

These results corroborate our prior observations on the uptake of *Candida albicans*, which is engaged by a highly similar cohort of phagocytic receptors[8]. Similarly, sphingolipids are known to be required for phagocytic infection of epithelial cells by *Pseudomonas aeruginosa* as demonstrated by Grassmé et al. in 2003 and *Neisseria gonorrhoeae*, as demonstrated by Hauck et al. in 2000[35,36].

In addition to the initial observations of defective internalization of Mtb by sphingolipid-deficient hosts, we present a possible mechanism through which sphingolipids enable the propagation of phagocytic signaling by coordinating the dynamics of phosphoinositide turnover. Upon engagement of phagocytic receptor to cognate ligand, Rho GTPases Rac1 and Cdc42 are activated and initiate the localized production of $PI_{(4,5)}P_2$. This local increase in the concentration of $PI_{(4,5)}P_2$ initiates F-actin polymerization at the base of the forming phagocytic cup, which drives pseudopodia around the particle. Concomitantly, the cyclic progression of the pseudopod necessitates F-actin disassembly and recycling: this process is driven by the conversion of $PI_{(4,5)}P_2$ to $PI_{(3,4,5)}P_3$ via PI3K at the trailing edge of the phagosomal cup[27]. Because we observe defects in the propagation of this signaling pathway beginning with the production of $PI_{(3,4,5)}P_3$, we believe that sphingolipids, and sphingomyelin in particular, are responsible for coordinating the necessary interactions between kinases and their phosphoinositide substrates. One candidate of particular interest for further investigation is PI3K, which may require interaction with or membrane tethering by sphingolipids (perhaps sphingomyelin specifically) at the site of phagocytic receptor engagement.

This study represents, to our knowledge, the first evidence for sphingolipids as regulators of phosphoinositide turnover during phagocytosis. However, prior work has shown that sphingolipids play roles in phosphoinositide signaling in other contexts. For example, phosphatidylinositol 4-phosphate (PI_4P) has been implicated in the transfer of ceramides from the ER to the Golgi by interacting with the ceramide transfer protein CERT[31]. Additionally, Capasso and colleagues showed that sphingomyelin production triggers dephosphorylation of PI_4P at the trans-Golgi as a negative feedback mechanism, suggesting regulatory interplay that maintains cellular levels of sphingomyelin[16].

As a whole, this study demonstrates that sphingolipids are key host factors in infection by *Mycobacterium tuberculosis*. Phagocytosis in this context represents a double-edged sword: while this immune process is critical for the clearance of many pathogenic particles, Mtb harnesses phagocytosis to gain entry to host cells and establish long-term survival. It may be possible to target a therapeutic to specifically block the interaction between Mtb and host lipids, but this will require more comprehensive understanding of how this lipid class enables Mtb pathogenicity. This study represents an important step in developing our knowledge of the underlying mechanisms of pathogenesis in *Mycobacterium tuberculosis* infection; we hope that such work contributes to the development of new strategies to fight this ancient pathogen.

Materials and Methods

Reagents.

Myriocin and fumonisin B1 were purchased from Cayman Chemical Company. 3-L-[^{14}C]serine was purchased from American Radioactivity. Phorbol 12-myristate 13-acetate (PMA) was purchased from BioLegend. 4% Paraformaldehyde was from Fisher Scientific. Alexa Fluor® 488 Phalloidin and Zymosan A (*S. cerevisiae*) BioParticles Alexa Fluor 594 conjugate were purchased from Thermo Fisher. Rabbit polyclonal antibody against phospho-PI3 Kinase p85 (Tyr458)/p55 (Tyr199) (p-PI3K) (#4228) was purchased from Cell Signaling Technology. Mouse Monoclonal antibody against GAPDH (ab8245) was purchased from Abcam. Anti-rabbit IgG HRP-linked antibody and anti-mouse IgG HRP-linked antibody were purchased from Cell Signaling.

Plasmids

Active (GTP-bound) Rac1/Cdc42 was detected with PAK(PBD)-YFP, a plasmid encoding the PBD of PAK fused to YFP[26]. $PI(_{4,5})P_2$ was detected with PH(PLCδ)-GFP, a plasmid encoding the PH domain of PLCδ fused to GFP (kindly provided by Grinstein). $PI(_{3,4,5})P_3$ levels were monitored by PH(AKT)-GFP, a plasmid encoding the PH domain of AKT fused to GFP[37].

The plasmids used for generation of lentivirus consists of the pCDH-CMV(-)-sgRNA plasmid, the psPAX2 plasmid (packaging) and pMD2.G plasmid (envelope). pCW-Cas9 lentivirus was purchased from Addgene.

Cell culture and drug treatment

THP-1, U937, Raw 264.7 and DC 2.4 cells were routinely cultured in RPMI medium supplemented with 10% FBS (Seradigm) and 1% Pen Strep (Gibco). HeLa cells were cultured in DMEM supplemented with 10% FBS and 1% Pen Strep. All cell lines were cultured at 37 °C and 5% CO_2.

THP-1 and U937 cells were differentiated to macrophages by 50ng/ml PMA for 1 day in RPMI medium supplemented with 10% FBS, after which the cells were treated with 5µM myriocin or fumonisin B1 for 3 days in RPMI supplemented with 10% FBS and 1%Pen Strep. RAW 264.7 and DC 2.4 cells were treated identically with myriocin and fumonisin B1.

Radio-active labeling and TLC

$5.0x10^5$ THP-1, U937, RAW 264.7, and DC 2.4 (both wildtype and Sptlc2-/-) cells were seeded into a well of a 6-well plate, differentiated and treated as described above (Cell culture and drug treatment). After 3 days of drug treatment the cells were labeled with 1µCi/ml of 3-L-[^{14}C]-serine for 4 hours in Opti-MEM supplemented with the appropriate drug concentration of myriocin and FB1 and incubated at 37°C. Cells were washed two times with PBS and lipid extraction was done following the Bligh and Dyer method[38]. The methanol/chloroform-lipid extracts were dried

by nitrogen gas. Dried lipids were re-dissolved in a few drops of chloroform/methanol (1:2, vol/vol) and loaded on a TLC plate. Lipids were separated by developing the TLC plate first in acetone and then in a mixture of chloroform, methanol and 25% ammonia solution (50:25:6, vol/vol/vol). Radiolabeled lipids were detected on a Storm 825 Phosphor-Imager (GE Healthcare).

Generation of Lentivirus.

Lentivirus production was performed as described previously[39]. Briefly, lentivirus was produced by co-transfection of HEK 293T cells with the pCDH-sgRNA/pCW-Cas9 and psPAX2 and pMD2.G. Transfection was performed with Lipofectamine 3000 (Thermo Fisher) according to manufacturer's instructions. Cells were cultured in DMEM supplemented with 10%FBS and the growth medium was replaced after 6 hours. 48 hours after transfection, lentivirus-containing supernatant was harvested, centrifuge for 5mins at 1250 rpm and filtered through a 0.45µm filter.

Generation of CRISPR/Cas9-mediated Sptlc2-/- Raw264.7 cell line.

Raw264.7 cells were infected with lentivirus (pCW-Cas9) encoding Cas9 cDNA, and were cultured in media containing 7 µg/mL of puromycin (Sigma Aldrich). Potential target sequences for CRISPR interference were found with the rules outlined in Mali et al. 2013[40]. The following seed sequences (CRISPR target sequences) preceding the PAM motif that were found in the exon of Sptlc2 gene were used: Sptlc2 #1 GAACGGCTGCGTCAAGAAC; Sptlc2 #2: AGCAGCACCGCCACCGTCG Potential off-target effects of the seed sequence were evaluated using the NCBI Mus musculus Nucleotide BLAST. Generation of CRISPR/Cas9-mediated Sptlc2-knockout Raw264.7 cell line was performed as previously described[39]. Briefly, CRISPR gBlock was designed to clone into the restriction enzymatic site NheI/BamHI of pCDH-CMV(-) (SBI; CD515B-1) as follows:

cacagtcagacagtgactcaGTGTCACAgctagcTTTCCCATGATTCCTTCATATTTGCATA-TACGATACAAGGCTGTTAGAGAGATAATTAGAATTAATTTGACTGTAAACACAAAGATATTAGTACAAAATACGTGACGTAGAAAGTAATAATTTCTTGGGTAGTTTGCAG-TTTTAAAATTATGTTTTAAAATGGACTATCATATGCTTACCGTAACTTGAAAGTATTTCGATTTCTTGGCTTTATATATCTTGTGGAAAGGACGAAACAC-CGnnnnnnnnnnnnnnnnn-nGTTTTAGAGCTAGAAATAGCAAGTTAAAATAAGGCTAGTCCGTTATCAACTTGAAAAAGTGGCACCGAGTCGGTGCTTTTTTTggatccTGTGCACAgtcagtcacagtcagtctac (n: CRISPR target sequences).

The gBlock was then digested using the restriction enzymes NheI and BamHI and ligated into pCDH-CMV(-) vector that was linearized by digesting with the same restriction enzyme.

The Cas9-inducible cells were infected with lentivirus carrying pCDH-CMV(-)-sgRNA, and were cultured in media containing 250 μg/mL of hygromycin B (Life Technology). To induce expression of Cas9, cells were treated with 2 μg/mL of doxycycline (Clontech) for 3–5 days. Clonal selection was performed by single cell dilution on 96-well plates. The individual colonies were collected and the expression of Sptlc2 was examined by western-blotting using Sptlc2 antibody.

U937 SGMS1 -/- cell lines

U937 SGSM1 -/- cells were kindly provided by Sebastian Virreira Winter (Max Plack Insitute) and the CRISPR/Cas9-mediated knock out cell lines were established as described in Winter et al., 2016[41].

Culturing of Mtb

Culturing and infection of Mtb was conducted in a Biosafety-level 3 laboratory following general safety guidelines. *M.tb* strain H37R, expressing constitutively mCherry, was cultured at 37°C in 7H9 Broth medium supplemented with 50µg/ml hygromycin B.

Infection of macrophages with *M.tb*

For infection of THP-1 and U937 cells, the cells were seeded into a SensoPlate™ 96-Well Glass-Bottom Plates (Greiner Bio-One) at a density of $1.5x10^4$ cells per well in RPMI supplemented with 10% FBS, 1% Pen Strep and 50ng/ml PMA at 37°C. One day after differentiation THP-1 cells were treated for 3 days with 5µM myriocin or 15µM fumonisin B1. Infection with *M.tb* was performed after three days of differentiation of U937 cells and three days of drug treatment of differentiated THP-1 cells. THP-1 and U937 cells were infected with a multiplicity of infection (MOI) of 10 in RPMI supplemented with 10% FBS for 4 hours at 37°C.

For infection of Raw264.7 and DC2.4 cells, $2.0x10^4$ cells / well were seeded 24 hours prior infection into a SensoPlate™ 96-Well Glass-Bottom Plates (Greiner Bio-One) and cultured in RPMI 10%FBS, 1%Pen Strep at 37°C. Raw264.7 and DC2.4 cells were infected with a MOI of 10 in RPMI supplemented with 10% FBS for 4 hours at 37°C.

After 4 hours *M.tb* containing supernatant was aspirated, cells were washed one time with PBS, and then fixed with 4% PFA over night at 4°C.

Microscopy

Confocal microscopy was performed using an LSM880 microscope (Zeiss, Oberkochen, Germany) using the PLAN APO for AiryScan 63x oil immersion objective, under the control of the Zeiss Zen Blue software. Spinning disk confocal (SDC) imaging was performed on a Yokogawa CSU-W1 SDC microscope (Nikon, Tokyo, Japan) using a 20x Plan Apo VC (NA 0.75) objective and a 60x Plan Apo VC (NA 1.4) oil immersion objective equipped with a Andor's Zyla sCMOS

camera under the control of the Nikon acquisition software and a stage motorized in X,Y. Live cell imaging was performed at 37°C and 5% CO_2 using multi-position imaging with automated focus at each time point. Representative images were analyzed and prepared using the FIJI software.

Further quantitative imaging was performed on a Keyence BZ-X700 all in one fluorescence microscope (Keyence Corporation, Osaka, Japan) using a SuperFluor 40.00xH oil immersion objective, and controlled using the Keyence BZ-X Viewer software. Image analysis and cell counting was performed using Keyence BZ-X Analyzer software and FIJI.

Phagocytosis assay

Phagocytosis assay was performed as previously described[42]. Briefly, fixed cells were washed twice with PBS and incubated in PBS for 15 min in Permeabilization Buffer (0.1% Triton X-100 and 1%BSA). Cells were stained with Phalloidin-Alexa 488 (Thermo Fisher) at a final concentration of 33nM for 60 min and washed one time with PBS. After the Phalloidin-staining, cells were stained with 1xDAPI for 10 mins and washed 3 times with PBS. THP-1 cells were then imaged using the SDC microscope (Nikon) with a 20x objective and the U937, Raw264.7 and DC2.4 cells were imaged with the Keyence BZ-X700 with a PlanFluor 20x objective. The parameters for imaging were kept the same for each sample. For image analysis either the Nikon or Keyence BZ-X Analyzer software was used. In brief: The outline of the cells was determined via the A488 signal (Phalloidin staining) and the number and area of mCherry (Mtb) signal in the A488 signal was detected by the program. In a second round the number of cells was determined by counting the nuclei via the DAPI staining. Number of bacteria (by mCherry-signal) inside the cell was divided by the number of cells analyzed to identify the phagocytosis efficiency.

Live imaging of phagocytosis

For transient transfection, Raw264.7 cells were seeded into a SensoPlate™ 96-Well Glass-Bottom Plates at a cell number of $1.0x10^4$ cells/well 24 hours prior transfection. Transfection was conducted with Lipofectamine 3000 (Thermo Fisher) according to manufacturer's instructions. Briefly, 100ng of plasmid DNA and 0.2µl of P3000 reagent were mixed in 5µl Opti-MEM and 0.33µl Lipofectamine 3000 was mixed in 5µl Opti-MEM. Both reagent dilutions were mixed together and allowed to sit for 15 min. The mix was then added directly to the appropriate well and mixed by swirling the plate gently.

For imaging, the growth medium was aspirated and replaced with RPMI without phenol red containing Zymosan A Bioparticles A595 (Thermo Fisher) at an MOI of 20. The 96-well plate were centrifuged at 1000rpm for one minute. The cells were imaged with the SDC microscope (Nikon) and 3-4 different spots per well were imaged at the same time for 60 min with capture intervals of 15 sec. The parameters for imaging were kept the same for each sample.

Live imaging analysis

Of live cell images, individual images were selected for further analysis if they captured a cell bound to a zymosan particle while maintaining a healthy morphology throughout the imaging timecourse.. Imaging analysis was performed using FIJI software[43]. The parameters for image processing were kept constant when comparing different data sets. The area of the phagosome was selected, cropped and opened in a new window. For the original image, the threshold was set automatically on the GFP-channel and for the threshold of the GFP-phagosome area, the threshold of the whole cell was multiplied by 1.5 to ensure that only an increase in signal is counted (GFP-threshold cell x 1.5 = GFP-threshold phagosome area). The threshold area at different time points was measured by the analyze-measure function of FIJI and the results were exported into Excel

(Microsoft). The values for the GFP-threshold of the phagosome area were divided by the values for the GFP-threshold of the whole cell at the corresponding time points.

Dectin-1 transfection and co-localization

Raw264.7 WT and *Sptlc2*$^{-/-}$ cells were seeded on glass coverslips in 12-well plates and grown to 70-90% confluency overnight. The next day, cells were transfected with pMXsIP Dectin-1-GFP using Lipofectamine 3000 (Invitrogen) according to the manufacturer's instructions. After 24 hrs, cells were washed three times with ice-cold PBS, kept on ice for 5 min, and inoculated with Alexa Fluor 594-conjugated zymosan in chilled serum-free DMEM at a ratio of 10 beads per cell. After centrifugation for 5 min at 250 x g and 4°C, cells were incubated for 5 min at 37°C, washed three times with ice-cold PBS to remove unbound zymosan, then fixed for 15 min with 4% paraformaldehyde.

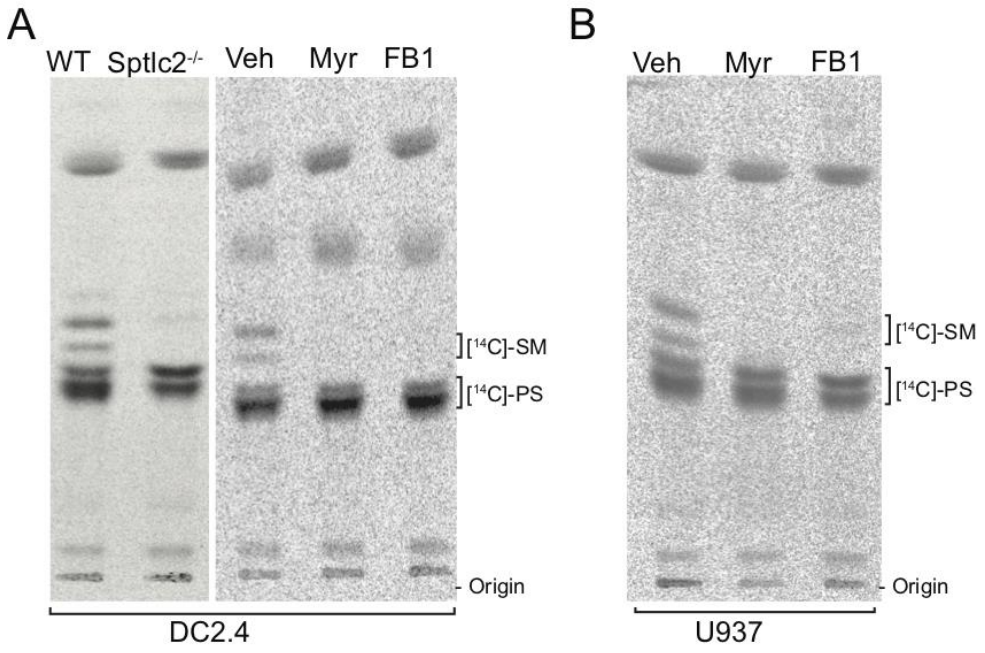

Supplemental Figure 1: *Sphingolipid depletion in DC 2.4 and U937 cells*

Thin-layer chromatography to visualize 3-L-[^{14}C]-serine incorporation into lipid species through autoradiography. (A) DC 2.4 cells of wildtype or Sptlc2-/- background, as well as wildtype treated for three days with vehicle control, 5µM myriocin, or 15µM fumonisin B1. (B) U937 cells treated for three days with vehicle control, 5µM myriocin, or 15µM fumonisin B1.

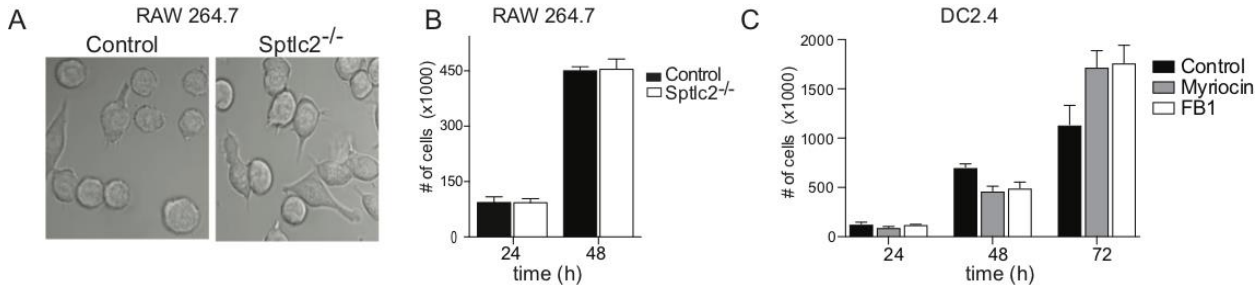

Supplemental Figure 2: *No phenotypes of morphology or growth rate are observed following sphingolipid depletion.*

Brightfield microscopy and proliferation assays to characterize effects of blocking sphingolipid biosynthesis. (A) RAW 264.7 macrophages visualized at 40x using brightfield microscopy. (B) RAW 264.7 wildtype and Sptlc2-/- cell growth after 24- and 48-hours in standard RPMI at 37°C in 5% CO_2 – as counted by hemacytometer in biological triplicate. (C) DC 2.4 cells untreated or treated with either 5µM myriocin or 15µM fumonisin B1 – as counted by hemacytometer in single biological replicate.

Citations

1. Daniel, T. M. The history of tuberculosis. *Respir. Med.* **100,** 1862–1870 (2006).
2. *Global tuberculosis report 2018.* (2018).
3. Korb, V., Chuturgoon, A. & Moodley, D. Mycobacterium tuberculosis: Manipulator of Protective Immunity. *Int. J. Mol. Sci.* **17,** 131 (2016).
4. Ouimet, M. *et al.* Mycobacterium tuberculosis induces the miR-33 locus to reprogram autophagy and host lipid metabolism. *Nat. Immunol.* **17,** 677–686 (2016).
5. Fine-Coulson, K., Reaves, B. J., Karls, R. K. & Quinn, F. D. The Role of Lipid Raft Aggregation in the Infection of Type II Pneumocytes by Mycobacterium tuberculosis. *PLoS One* **7,** (2012).
6. Thompson, C. R. *et al.* Sphingosine Kinase 1 (SK1) Is Recruited to Nascent Phagosomes in Human Macrophages: Inhibition of SK1 Translocation by Mycobacterium tuberculosis. *J. Immunol.* **174,** 3551–3561 (2005).
7. Levin, R., Grinstein, S. & Schlam, D. Phosphoinositides in phagocytosis and macropinocytosis. *Biochim. Biophys. Acta - Mol. Cell Biol. Lipids* **1851,** 805–823 (2015).
8. Tafesse, F. G. *et al.* Disruption of Sphingolipid Biosynthesis Blocks Phagocytosis of Candida albicans. *PLoS Pathog.* **11,** 1–27 (2015).
9. Malik, Z. A. *et al.* Cutting Edge: Mycobacterium tuberculosis Blocks Ca2+ Signaling and Phagosome Maturation in Human Macrophages Via Specific Inhibition of Sphingosine Kinase. *J. Immunol.* **170,** 2811–2815 (2003).
10. El Alwani, M., Wu, B. X., Obeid, L. M. & Hannun, Y. A. Bioactive sphingolipids in the modulation of the inflammatory response. *Pharmacol. Ther.* **112,** 171–183 (2006).
11. Hla, T. & Dannenberg, A. J. Sphingolipid Signaling in Metabolic Disorders. *Cell Metab.*

16, 420–434 (2012).

12. Taha, T. A., Mullen, T. D. & Obeid, L. M. A house divided: Ceramide, sphingosine, and sphingosine-1-phosphate in programmed cell death. *Biochim. Biophys. Acta - Biomembr.* **1758,** 2027–2036 (2006).

13. Hakomori, S. I. & Igarashi, Y. Functional role of glycosphingolipids in cell recognition and signaling. *J. Biochem.* **118,** 1091–1103 (1995).

14. Hannun, Y. A. & Obeid, L. M. The ceramide-centric universe of lipid-mediated cell regulation: Stress encounters of the lipid kind. *J. Biol. Chem.* **277,** 25847–25850 (2002).

15. Snider, A. J., Alexa Orr Gandy, K. & Obeid, L. M. Sphingosine kinase: Role in regulation of bioactive sphingolipid mediators in inflammation. *Biochimie* **92,** 707–715 (2010).

16. Capasso, S. *et al.* Sphingolipid metabolic flow controls phosphoinositide turnover at the trans -Golgi network. *EMBO J.* **36,** 1736–1754 (2017).

17. Kinoshita, M., Suzuki, K. G. N., Murata, M. & Matsumori, N. Evidence of lipid rafts based on the partition and dynamic behavior of sphingomyelins. *Chem. Phys. Lipids* **215,** 84–95 (2018).

18. García-Arribas, A. B., Alonso, A. & Goñi, F. M. Cholesterol interactions with ceramide and sphingomyelin. *Chem. Phys. Lipids* **199,** 26–34 (2016).

19. Hinkovska-Galcheva, V., Boxer, L., Mansfield, P. J., Schreiber, A. D. & Shayman, J. A. Enhanced Phagocytosis through Inhibition of de Novo Ceramide Synthesis. *J. Biol. Chem.* **278,** 974–982 (2003).

20. Gatfield, J. & Pieters, J. Essential role for cholesterol in entry of mycobacteria into macrophages. *Science* **288,** 1647–50 (2000).

21. Hanada, K. Serine palmitoyltransferase, a key enzyme of sphingolipid metabolism.

Biochim. Biophys. Acta **1632,** 16–30 (2003).

22. Gault, C., Obeid, L. & Hannun, Y. An overview of sphingolipid metabolism: from synthesis to breakdown Introduction to Sphingolipid Metabolism. *Adv Exp Med Biol* **688,** 1–23 (2010).

23. Leier, H. C., Messer, W. B. & Tafesse, F. G. Lipids and pathogenic flaviviruses : An intimate union. 1–7 (2018). doi:https://doi.org/10.1371/journal.ppat.1006952

24. Meivar-Levy, I., Sabanay, H., Bershadsky, A. D. & Futerman, A. H. The Role of Sphingolipids in the Maintenance of Fibroblast Morphology. *J. Biol. Chem.* **272,** 1558–1564 (2002).

25. Mao, Y. & Finnemann, S. C. Regulation of phagocytosis by Rho GTPases. *Small GTPases* **6,** 89–99 (2015).

26. Hoppe, A. D. & Swanson, J. A. Cdc42, Rac1, and Rac2 Display Distinct Patterns of Activation during Phagocytosis. *Mol. Biol. Cell* **15,** 3509–3519 (2004).

27. Schlam, D. *et al.* Phosphoinositide 3-kinase enables phagocytosis of large particles by terminating actin assembly through Rac/Cdc42 GTPase-activating proteins. *Nat. Commun.* **6,** 8623 (2015).

28. Underhill, D. M. Macrophage recognition of zymosan particles. *J. Endotoxin Res.* **9,** 176–180 (2003).

29. Rothfuchs, A. G. *et al.* Dectin-1 Interaction with Mycobacterium tuberculosis Leads to Enhanced IL-12p40 Production by Splenic Dendritic Cells. *J. Immunol.* **179,** 3463–3471 (2007).

30. Queval, C. J., Brosch, R. & Simeone, R. The Macrophage: A Disputed Fortress in the Battle against Mycobacterium tuberculosis. *Front. Microbiol.* **8,** (2017).

31. Hanada, K. *et al.* Molecular machinery for non-vesicular trafficking of ceramide. *Nature* **426,** 803–809 (2003).

32. Marshall, J. G. *et al.* Restricted accumulation of phosphatidylinositol 3-kinase products in a plasmalemmal subdomain during Fcγ receptor-mediated phagocytosis. *J. Cell Biol.* **153,** 1369–1380 (2001).

33. Subbaiah, P. V. & Sargis, R. M. Sphingomyelin: A natural modulator of membrane homeostasis and inflammation. *Med. Hypotheses* **57,** 135–138 (2001).

34. Goodridge, H. S. *et al.* Activation of the innate immune receptor Dectin-1 upon formation of a 'phagocytic synapse'. *Nature* **472,** 471–475 (2011).

35. Grassmé, H. *et al.* Host defense against Pseudomonas aeruginosa requires ceramide-rich membrane rafts. *Nat. Med.* **9,** 322 (2003).

36. Hauck, C. R. *et al.* Acid sphingomyelinase is involved in CEACAM receptor-mediated phagocytosis of Neisseria gonorrhoeae. *FEBS Lett.* **478,** 260–266 (2000).

37. Feng, S. *et al.* A Rapidly Reversible Chemical Dimerizer System to Study Lipid Signaling in Living Cells. *Angew. Chemie Int. Ed.* **53,** 6720–6723 (2014).

38. BLIGH, E. G. & DYER, W. J. A rapid method of total lipid extraction and purification. *Can. J. Biochem. Physiol.* **37,** 911–7 (1959).

39. Tafesse, F. G. *et al.* GPR107, a G-protein-coupled Receptor Essential for Intoxication by Pseudomonas aeruginosa Exotoxin A, Localizes to the Golgi and Is Cleaved by Furin. *J. Biol. Chem.* **289,** 24005–24018 (2014).

40. Mali, P. *et al.* RNA-guided human genome engineering via Cas9. *Science* **339,** 823–6 (2013).

41. Virreira Winter, S., Zychlinsky, A. & Bardoel, B. W. Genome-wide CRISPR screen

reveals novel host factors required for Staphylococcus aureus α-hemolysin-mediated toxicity. *Sci. Rep.* **6,** 24242 (2016).

42. Rashidfarrokhi, A., Richina, V. & Tafesse, F. G. Visualizing the Early Stages of Phagocytosis. *J. Vis. Exp.* (2017). doi:10.3791/54646

43. Schindelin, J. *et al.* Fiji: an open-source platform for biological-image analysis. *Nat. Methods* **9,** 676–682 (2012).

SupplementaryMovie1 WT PBD(PAK)-YFP

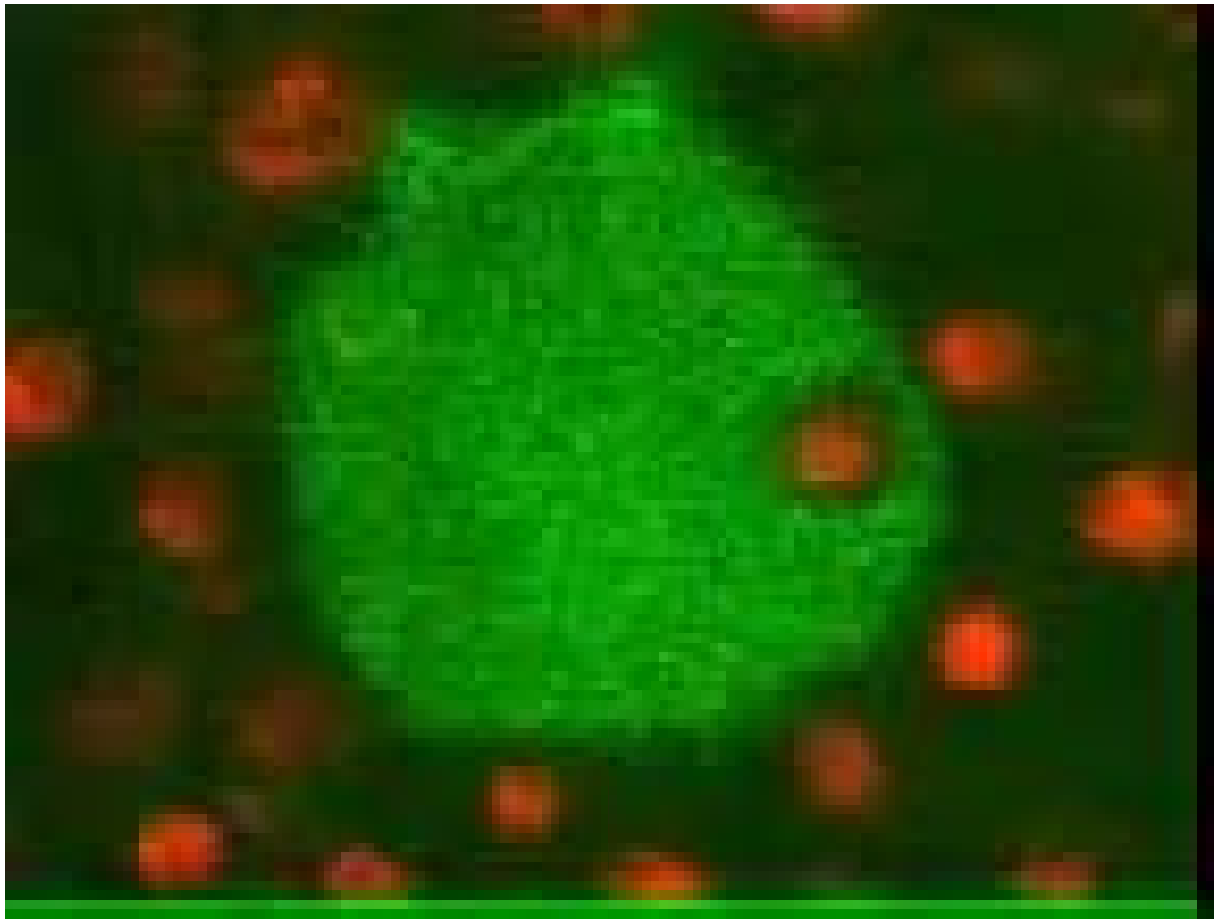

SupplementaryMovie2 Sptcl2-/-
PBD(PAK)-YFP

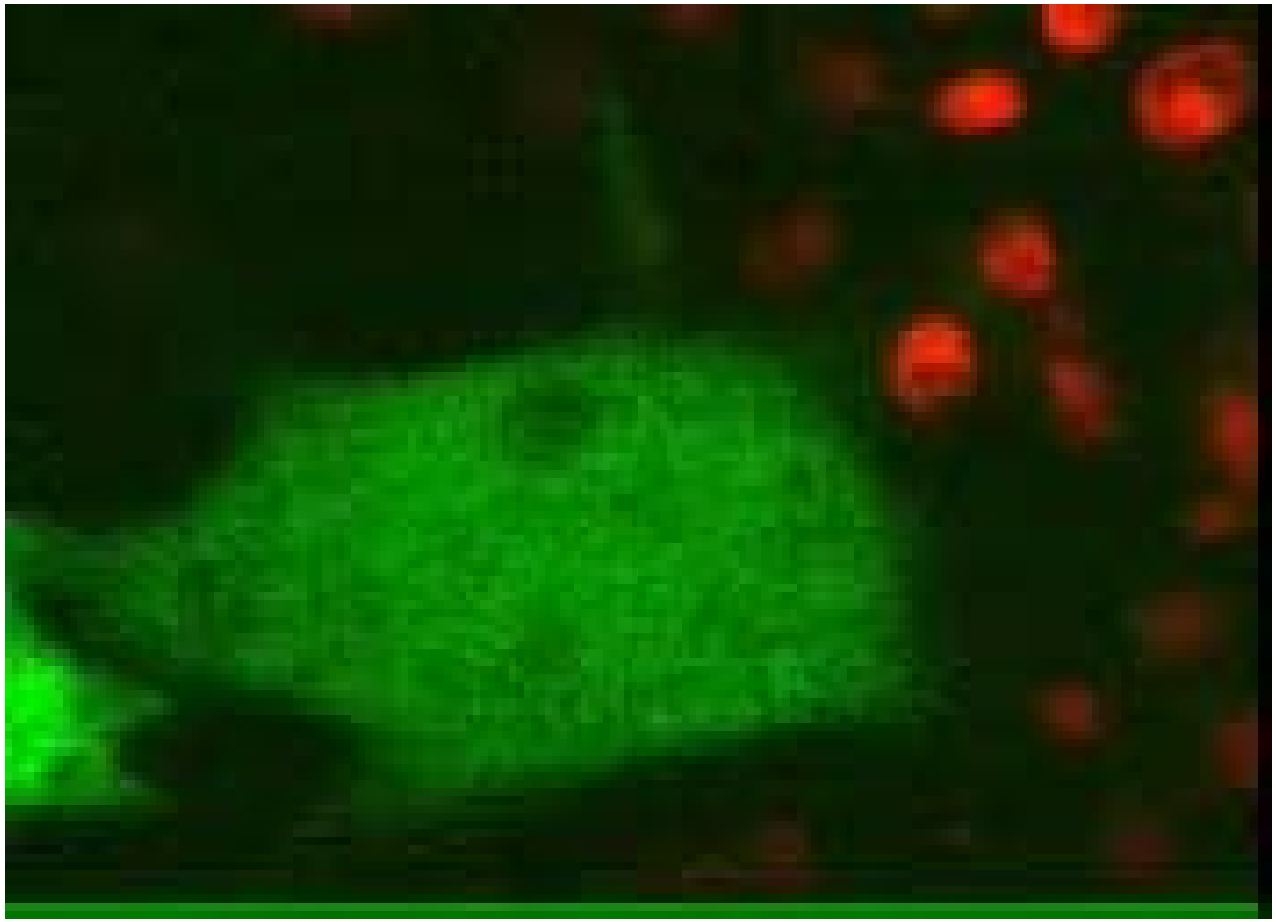

SupplementaryMovie3 WT PH(PLCdelta)-GFP

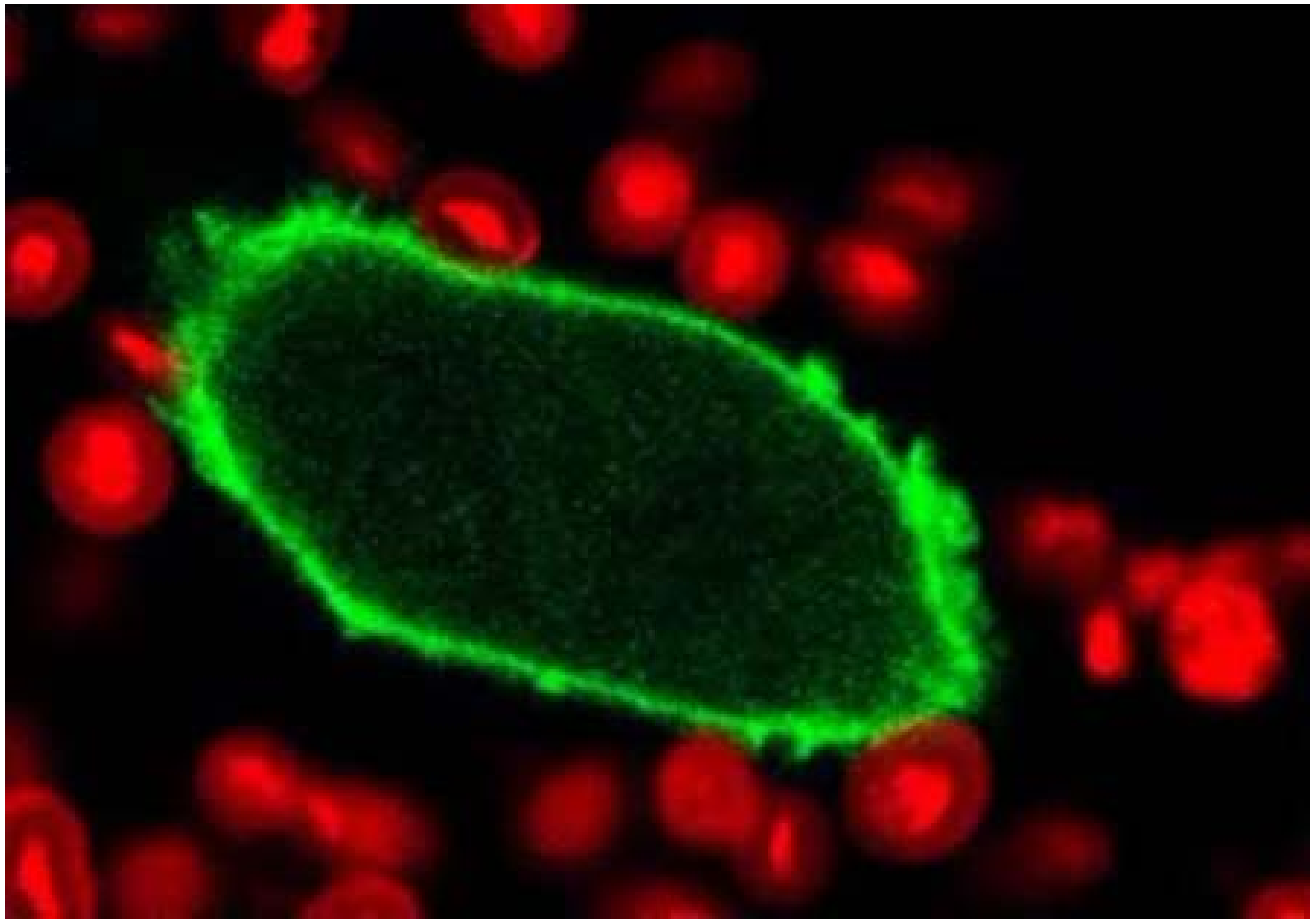

SupplementaryMovie4 Sptcl2-/-
PH(PLCdelta)-GFP

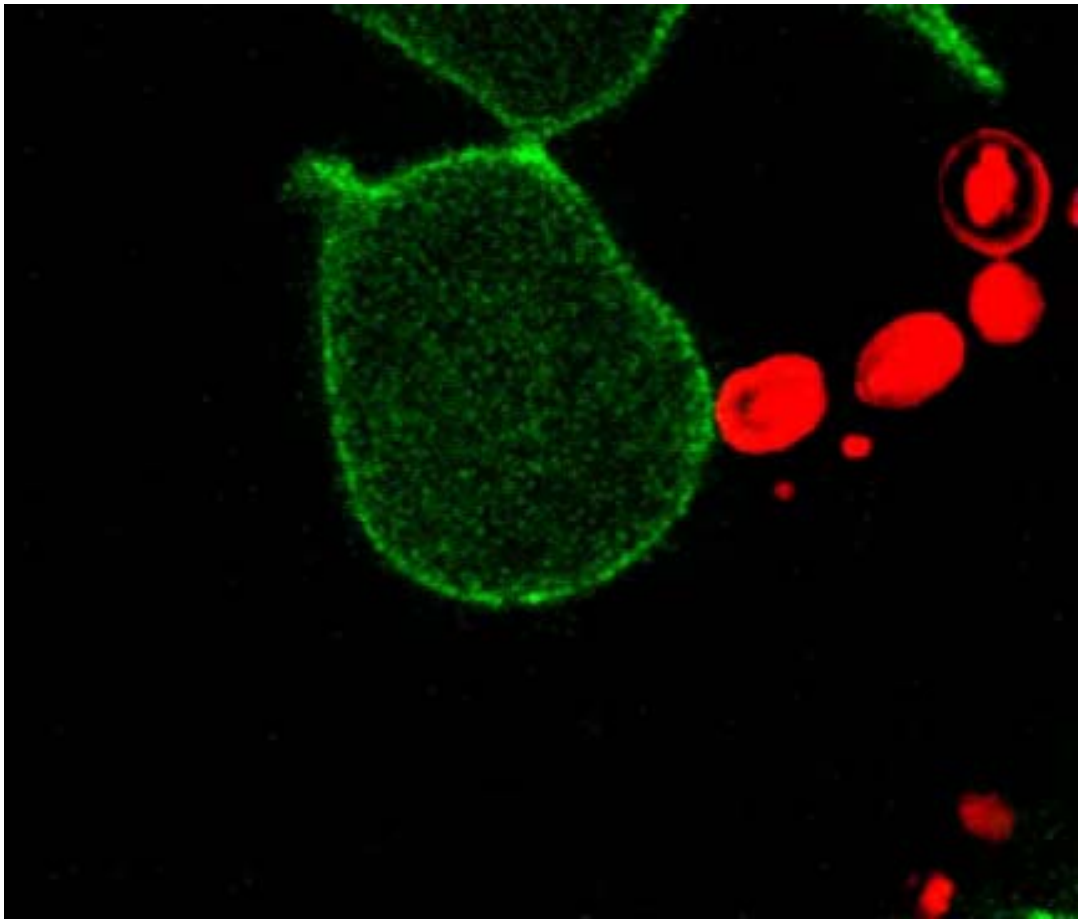

SupplementaryMovie5 WT PH(AKT)-GFP

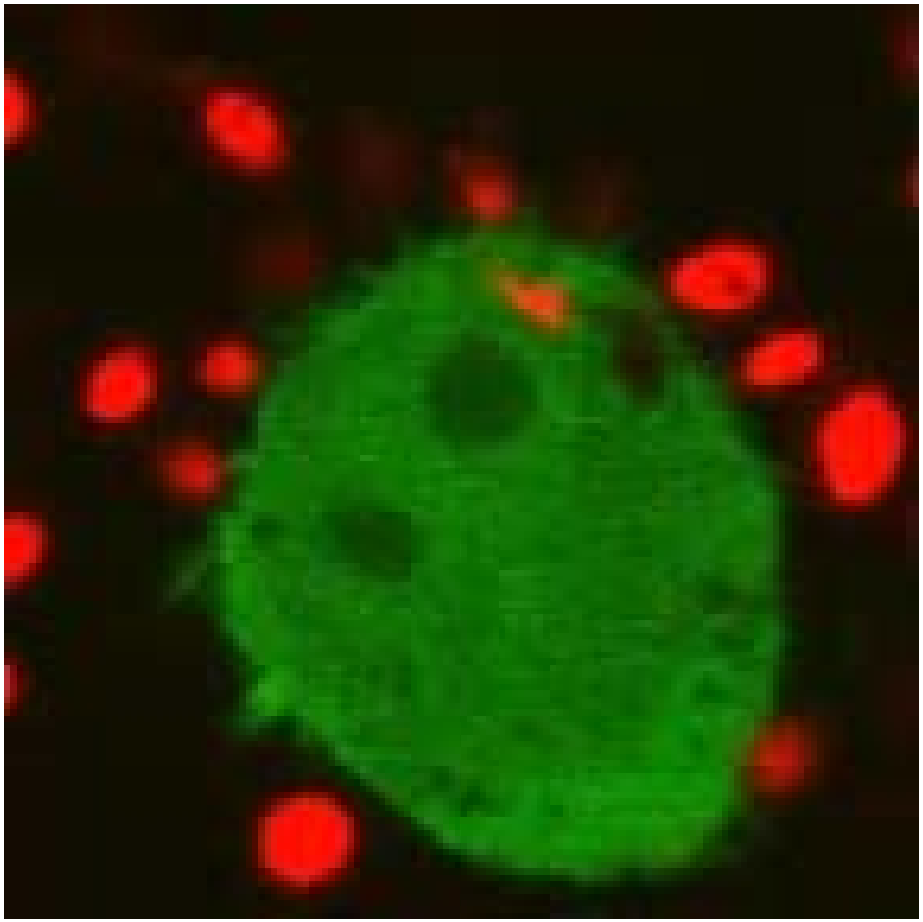
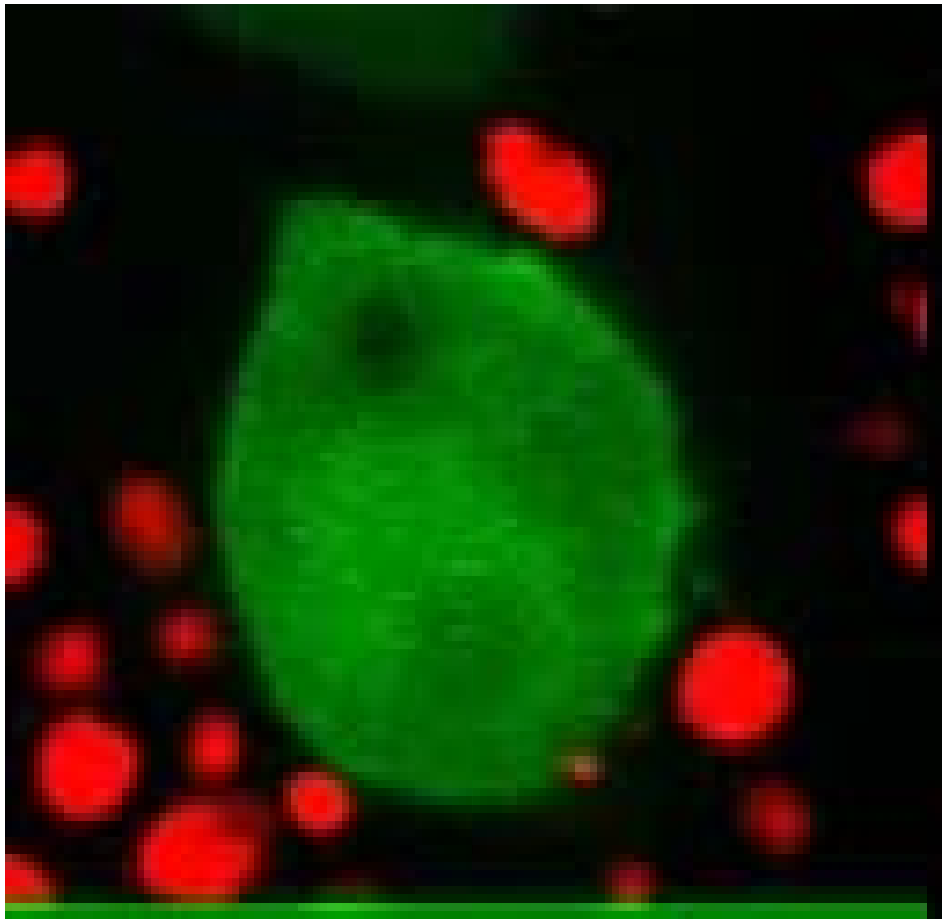
SupplementaryMovie6 Sptcl2-/-
PH(AKT)-GFP